Shear-induced self-diffusion of inertial particles in a viscous fluid

Micheline Abbas,[1,2] Eric Climent,[1,*] and Olivier Simonin[2]
[1]*Laboratoire de Génie Chimique, CNRS-INPT-UPS UMR 5503, 5, Rue Paulin Talabot, 31106 Toulouse, France*
[2]*Institut de Mécanique des Fluides de Toulouse, CNRS-INPT-UPS UMR 5502, 1, Allée du Professeur Camille Soula, 31400 Toulouse, France*
(Received 11 July 2008; revised manuscript received 29 October 2008; published 26 March 2009)

We propose a theoretical prediction of the self-diffusion tensor of inertial particles embedded in a viscous fluid. The derivation of the model is based on the kinetic theory for granular media including the effects of finite particle inertia and drag. The self-diffusion coefficients are expressed in terms of the components of the kinetic stress tensor in a general formulation. The model is valid from dilute to dense suspensions and its accuracy is verified in a pure shear flow. The theoretical prediction is compared to simulations of discrete particle trajectories assuming Stokes drag and binary collisions. We show that the prediction of the self-diffusion tensor is accurate provided that the kinetic stress components are correctly predicted.

DOI: 10.1103/PhysRevE.79.036313 PACS number(s): 47.55.Kf, 66.10.C−, 82.70.Kj, 83.10.Rs

I. INTRODUCTION

Shear-induced self-diffusion has been a long-standing topic of research. This phenomenon is a subtle combination of the microstructure evolution within the suspension and its rheology. Self-diffusion has been a point of interest for many works dedicated to a better understanding of fundamental phenomena involved in industrial applications such as fluidized beds, separation, and mixing processes. The self-diffusion of similar particles results from particle/particle and particle/fluid interactions and may occur in a suspension macroscopically homogeneous. In this paper, we aim at investigating theorically and numerically the long-time self-diffusion of monodisperse particles with finite inertia accounting for collisions and Stokes drag. The relative motion of the particles is forced by a simple shear flow and eventually by the overall agitation of the suspension. We assume that the particulate Reynolds number is small and neglect the effects of Brownian motion (macroscopic particles). The particle inertia is characterized by the Stokes number [$\mathrm{St}=\tau_p/\tau_f$]. This dimensionless number compares the fluid characteristic time scale τ_f ([$\tau_f=\dot{\gamma}^{-1}$] where $\dot{\gamma}$ is the shear rate of the carrying fluid flow) and the viscous relaxation time scale of the particle [$\tau_p=2/9(\rho_p a^2/\mu_f)$] (where ρ_p and a stand, respectively, for the particle density and radius; μ_f is the dynamic fluid viscosity). Matching simultaneously both conditions of low Reynolds and moderate to high Stokes numbers corresponds to solid millisized particles [diameter of $O(0.1-1)$ mm] suspended in a gas flow sheared at a typical rate $\approx 10\ \mathrm{s}^{-1}$. Due to the large contrast of density, gas-particle suspensions are obviously influenced by buoyancy effects. This particular aspect of the coupling between shear-induced agitation and mean slip due to gravity has been addressed in [1]. In the present study, we chose to neglect the mean settling of the suspension in order to highlight the effect of shear. Indeed, predicting the response of a sheared suspension is a keystone of more complex physical configurations (at small scales, turbulent flows may be regarded as coherent structures with different shear rates). The effect of the mean slip due to buoyancy may complicate the analysis as local gradients of solid concentration provoke large scale motions in the suspension that consequently contribute to the kinetic stress tensor. Also, momentum transfer in the horizontal directions is not directly related to the mean vertical contribution of gravity. As we seek to verify the validity of a theoretical prediction of the long-time diffusion of moderately inertial particles suspended in a gas when gravity is neglected, experiments may not be envisageable. Therefore we carried out numerical simulations based on a discrete element method.

When $\mathrm{St}\ll 1$ (suspension of small solid particles in a highly viscous fluid), physical collisions of smooth particles are unlikely as hydrodynamic interactions (lubrication repulsion) prevent actual contacts in a finite time. In the regime of highly inertial disperse phase ($\mathrm{St}\to\infty$), particles fly along straight lines between successive collisions. This corresponds to dry granular materials. When the Stokes number is moderate, the particles experience a significant drag forcing them to recover the fluid pathlines in a characteristic time τ_p. In this latter complex case, three characteristic time scales control the dynamics of the suspension: τ_p, τ_f, and τ_c (the typical time spent by a given particle between two consecutive collisions). Energy dissipation occurs through inelastic collisions and drag work.

The self-diffusion of particles has been thoroughly studied in the two asymptotic cases of low and high inertia. On one hand, when $\mathrm{St}\ll 1$ (the hydrodynamic interactions are dominant), several authors [2–4] have investigated long-time self-diffusion of solid particles by numerical or experimental approaches. The particle diffusivity is related to the particulate velocity fluctuations and the random motion occurring after multiple particle encounters. Theoretical prediction for self-diffusion due to three-body hydrodynamic interactions was proposed by [5] in the limit of dilute suspensions. For moderately concentrated suspensions, multibody interactions prevail and this leads to a dramatic complication of the mathematical formulation. Brady and Morris [6] have determined the coefficients of self-diffusion induced by pure hydrody-

*climent@imft.fr

namic interactions with and without additional short-range forces. The authors found that the self-diffusion coefficient is proportional to $\gamma a^2\phi$ in the dilute limit and to $\gamma a^2\phi g^{\infty}(2;\phi)$ in the high concentration limit (where ϕ is the solid volume fraction and $g^{\infty}(2;\phi)$ is the pair distribution at contact). The contribution of $g^{\infty}(2;\phi)$ becomes dominant when increasing the particle concentration.

On the other hand, when $\mathrm{St}\to\infty$, the behavior of highly agitated granular materials was approximated to the behavior of a dense gas. In this context, self-diffusion coefficients were predicted using the kinetic theory for rapid granular flow [7]. When the suspension is isotropically agitated, the basic result is a single diffusion coefficient D [Eq. (1)] expressed in terms of the restitution coefficient e, the collision time τ_c, and the level of the particle velocity fluctuations T (often called granular temperature),

$$D=\frac{3}{(1+e)}\tau_c T. \tag{1}$$

Under the same assumption of negligible drag effects, the shear-induced self-diffusion was investigated by [8] (as a function of e and ϕ) using discrete particle simulations. The author emphasized that shear-induced self-diffusion has to be characterized by an anisotropic tensor D_{ij} instead of a unique dispersion coefficient. Reference [9] determined analytically D_{ij} within the framework of the kinetic theory and clearly stated the dependence of the diffusion coefficients on the components of the particulate kinetic stress tensor T_{ij} (instead of the particle agitation $T=T_{ii}/3$; see definitions in Sec. III). However, little attention has been paid to the influence of the drag force (moderate St) on the self-diffusion of particles. Reference [10] considered the effect of the hydrodynamic drag while they theoretically predicted the self-diffusion coefficient of a dilute suspension under isotropic agitation. Their result is similar to Eq. (1) with a prefactor depending on both τ_p and τ_c. Following their approach, we suggest to generalize the dispersion model from dilute to dense suspensions accounting for the dependence of self-diffusion on the kinetic stress tensor components. The theoretical prediction is validated by numerical simulations of discrete particle trajectories in a pure shear flow.

II. SIMULATION METHOD

In the simulations, we assume that the presence of the particles does not perturb the carrying fluid flow. The velocity profile is a linear shear $\boldsymbol{u}(\boldsymbol{x})=\gamma x_2\mathbf{i}_1$ where $\mathbf{i}_1$ is the unit vector in the flow direction. Particles are initially seeded at random positions within the domain of computation and their velocities are equal to the local velocity of the fluid. The numerical scheme is based on a classic discrete particle simulation (DPS) method. Each particle experiences the Stokes drag force which models the interaction with the fluid. The Lagrangian tracking of the discrete phase is carried out by solving Newton's law for the motion of each particle written in dimensionless form: $\frac{d\mathbf{v}}{dt}=\frac{1}{\mathrm{St}}(\mathbf{v}-\boldsymbol{u})$ and $\frac{d\mathbf{x}}{dt}=\mathbf{v}$. Only binary collisions are considered according to the kinetic theory assumptions. The detection of collisions is performed

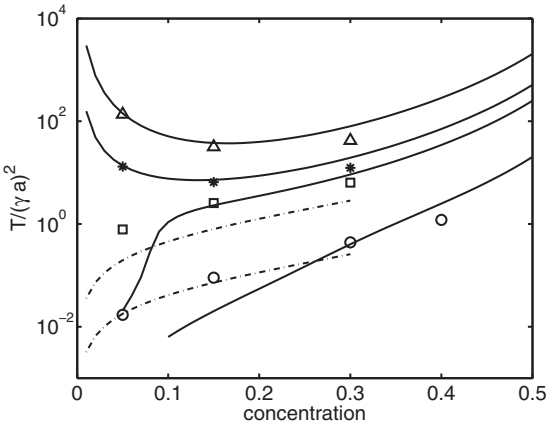

FIG. 1. $T/(\gamma a)^2$ vs ϕ. Symbols: numerical results (△, ∗, □, ○ correspond, respectively, to St=10, 5, 3.5, and 1). Solid lines: prediction of the ignited theory (from top to bottom: St=10, 5, 3.5 and 1). Dashed-dotted lines: quenched theory of [20] multiplied by $2g_0$ (upper: St=3.5, lower: St=1).

at the beginning of each time step. For each collision, impact velocities and positions are determined at the exact time of the collision (between t and $t+dt$). Then, the postcollision quantities are calculated using the assumption of elastic rebound ($e=1$) and the new positions and velocities are updated at the time $t+dt$ corresponding to the next time step. The simulations are performed in a triperiodic cubic domain of width ($L/a\approx 48$). The particle size and the width of the domain are kept constant throughout all the simulations and various volumetric concentrations of the suspension are investigated when varying the total number of particles (the typical number of particles is 4000 for $\phi=15\%$). Periodic boundary conditions in the three directions of the domain helped preserving the homogeneity of the suspension under shear. Of course, a particular treatment is operated when a particle crosses the boundary $x_2=0$ (resp. $x_2=L$) as the shear contribution γL has to be added (resp. removed) to the particle velocity component u_1. The ratio L/a is not very large in order to prevent the formation of dense layers populated with particles [11], and not too small allowing each particle to experience many collisions along its trajectory between two boundaries. A fixed time step is selected using the condition $dt=\min(\tau_p,\tau_c)/50$. This condition provides an accurate resolution of the two following phenomena: the trajectories of weakly inertial particles have to recover the fluid velocity on a time scale τ_p and for highly inertial particles the time scale between two consecutive collisions is τ_c. The collision time scale is calculated *a priori* using either the theoretical prediction based on the kinetic theory assuming that the suspension is strongly agitated $\tau_c=\frac{a\sqrt{\pi}}{12\phi g_0\sqrt{T}}$ [7] (T corresponding to the solid lines of Fig. 1) or the estimate based on the characteristic time of particle encounters due to the shear flow $\tau_c=\frac{\pi}{16\phi\gamma}$. In a very dilute suspension, two additional conditions must be satisfied to enforce a relevant selection of dt. First, the time step should be much smaller than a time scale based on the velocity fluctuation $a/\sqrt{T}$, especially at high particle inertia. This constraint will prevent any omission of collision and is a strong limitation of dt for highly agitated regimes. Second, a particle should experience

several collisions before crossing the entire domain of simulation. The condition $\tau_c \ll \frac{L}{\sqrt{T}}$ prevents an unrealistic increase of the suspension agitation energy due to the summation of $L\gamma$ velocity increments (or decrements) when particles are crossing the bottom (resp. upper) boundary conditions. Statistical Lagrangian quantities are formed along the trajectories after the system has reached the steady state. Typically, each particle may experience at least 600 collisions during the time average. The long-time self-diffusion regime requires a sufficient time of simulation to observe the diffusive temporal evolution of the mean-square displacement [3]. The effect of long-range and lubrication hydrodynamic interactions in Stokes flows between the inertial particles is neglected in our simulations. Reference [12] showed that this effect can be simply modeled by a correction factor $R_{\mathrm{diss}}(\phi,\epsilon)$ related to the viscous energy dissipation (ϵ is a threshold separation length of the particles where the lubrication approximation breaks down). Including the direct hydrodynamic interactions would be similar to a reduction in the overall Stokes number of the suspension flow, replacing St by $\mathrm{St}/R_{\mathrm{diss}}$. In [12], they determined R_{diss} from simulations based on the Stokesian dynamics approach. This scaling factor increases with ϕ and decreases with ϵ. They found that $2.2 \leq R_{\mathrm{diss}} \leq 15$ for $\epsilon=0.01$ $(0.01 \leq \phi \leq 0.5)$ and $2.2 \leq R_{\mathrm{diss}} \leq 7$ when $\epsilon=0.1$. Our simulations without direct hydrodynamic interactions correspond to $R_{\mathrm{diss}}=1$.

III. AGITATION AND KINETIC STRESS

Self-diffusion is intimately related to the level of velocity fluctuations of the disperse phase. Therefore, we first characterized the solid phase averaged agitation $T=\langle C_i C_i\rangle/3$ [where $\boldsymbol{C}=\boldsymbol{c}-\boldsymbol{U}_p(\boldsymbol{x})$ is the local velocity fluctuation relative to the average particulate phase velocity $\boldsymbol{U}_p(\boldsymbol{x})=\gamma x_2 \mathbf{i}_1$] and the kinetic stress tensor $T_{ij}=\langle C_i C_j\rangle$. Together with the collisional stress (momentum transfer due to collisions), they characterize the rheology of a flowing granular material. The rheology of dry granular flows was studied by means of both experimental [13,14] and numerical [8,11,15] investigations. Theoretical predictions based on the kinetic theory [7,16–18] rely on a statistical approach for an ensemble of hard spheres. When the particle inertia is finite, the theory used for dry granular material can be generalized with additional terms due to the drag force [7]. Hence, the microscopic transport equation is now written as

$$\frac{\partial f}{\partial t}+\frac{\partial (c_i f)}{\partial x_i}+\frac{\partial}{\partial c_i}\left(\frac{c_i-u_i}{\tau_p}f\right)=\frac{\partial_c f}{\partial t}, \tag{2}$$

where the probability density function $f(\boldsymbol{c},\boldsymbol{x})$ depends on the position and velocity in the phase space ($\boldsymbol{x}$ and $\boldsymbol{c}$). The action of the carrying fluid is accounted for through the particle acceleration $(\boldsymbol{c}-\boldsymbol{u})/\tau_p$ where $\boldsymbol{u}$ is the unperturbed fluid velocity. $\partial_c f/\partial t$ is the temporal rate of change of f due to the collisions.

Assuming perfectly elastic collisions ($e=1$), the equilibrium state occurs when the energy input from the carrying fluid balances the drag induced dissipation. Solving the system of equations derived from Eq. (2) for the second-order moments of the velocity fluctuation (see [18]) leads to a theoretical prediction of particle fluctuation level. However, the critical point of the theory is the prescribed analytic form of $f(\boldsymbol{c},\boldsymbol{x})$ for determining the collisional rate of change of any dynamic quantity, particularly the components of the kinetic stress tensor. In a highly agitated regime of granular flow resulting from homogeneous shear, [16] proposed to approximate f by a deviated Maxwellian distribution

$$f(\boldsymbol{c},\boldsymbol{x})=\left\{1+\frac{T_{ij}-T}{2T}\frac{\partial^2}{\partial c_i\,\partial c_j}\right\}f_0(\boldsymbol{c},\boldsymbol{x}) \tag{3}$$

where $[f_0(\boldsymbol{c},\boldsymbol{x})=\frac{n}{2\pi T^2}\exp(-\frac{C^2}{2T})]$ is the Maxwellian distribution that holds under the equilibrium assumption where n is the particle number density. The second-order term in the deviated Maxwellian remains only in the case of an anisotropic kinetic stress tensor $T_{ij}=\langle C_i C_j\rangle$. Reference [18] used the deviated Maxwellian function for calculating the collisional rate of change of dynamic quantities for $\mathrm{St}\to\infty$, whereas [12,19] used a similar approach to predict T and T_{ij} for particles of moderate inertia embedded in a viscous fluid in the particular case of a pure shear flow. When both the suspension concentration ϕ and the particle inertia are low, it is much less obvious to select an adequate shape of f because particles have very weak velocity fluctuations as they are most likely to follow the fluid streamlines $[\tau_p \ll \tau_c]$. Reference [20] proposed to close the equations assuming a Dirac delta function $[f(C)=\delta(C)]$; this peculiar regime is called by Tsao and Koch [20] "the quenched state" as opposed to the "ignited theory" for agitated systems. However their formulation holds only for dilute particulate flows since they considered that the two-particle distribution function in the collisional terms obeys $f^{(2)}(\boldsymbol{c}_A,\boldsymbol{c}_B)=f(\boldsymbol{c}_A)f(\boldsymbol{c}_B)$ ($\boldsymbol{c}_A$ and $\boldsymbol{c}_B$ are the colliding particle velocities). For moderate ϕ, the enhancement of the probability to find close particle pairs could be accounted for, similarly to the theory for dense gases [7], by assuming $f^{(2)}(\boldsymbol{c}_A,\boldsymbol{c}_B)=g_0 f(\boldsymbol{c}_A)f(\boldsymbol{c}_B)$. g_0 depends only on ϕ in a homogeneous suspension and is given by the peak value of the radial distribution of pairs at contact ($r=2a$). An extension of Tsao and Koch's approach allowed to point out that a factor 2 is missing in the collision terms (Eqs. 4.8 and 4.9 of [20]).

Simulation results are compared to the theoretical prediction of the particle agitation in Fig. 1 for $1 \leq \mathrm{St} \leq 10$ and $5 \leq \phi \leq 30\%$. The level of the mean agitation T is very well predicted by the ignited theory [12,19] for high St or moderate to high ϕ. At low St and ϕ, the prediction is significantly improved when we used the model based on the quenched regime assumption. The transition from a low to high agitation regime is closely related to the predominance of collisions accordingly with the relation $[\tau_p/\tau_c > 1]$. In a shear flow, the kinetic stress tensor is not isotropic as differences of normal components arise at low St and ϕ (i.e., $T_{ij} \neq T\delta_{ij}$). Figure 2 shows the difference between the stress in the flow direction T_{11} and the average stress T. The normal stress difference (for all directions) is large when the particle relaxation time becomes of the order of the collision time. When the particle inertia increases, the anisotropy decreases

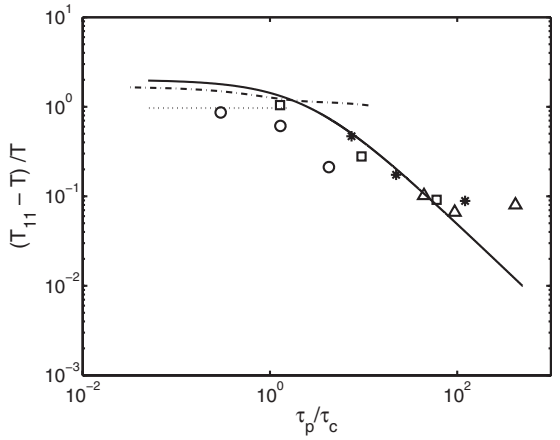

FIG. 2. Kinetic stress difference $(T_{11}-T)/T$ vs τ_p/τ_c. Solid line: theoretical prediction for the ignited state. Dotted and dotted-dashed lines: quenched theory for St=1 and St=3.5, respectively. Symbols: numerical results (△, ∗, □, ○ correspond, respectively, to St=10, 5, 3.5, and 1).

strongly with the Stokes number and eventually becomes negligible for a dry granular material (Newtonian behavior).

IV. LONG-TIME SELF-DIFFUSION

A. Theoretical modeling

Let us consider a homogeneous suspension of similar particles (size and density) and assume that a given number of these particles are labeled in some way. For instance, a number of particles might be colored in red. In an Eulerian framework, let n_r be the spatial distribution of the mean number density of the red particles in the suspension. If the red particles are not homogeneously distributed, $n_r(\boldsymbol{x})$ may have a spatial gradient although the overall mean number density n related to all the particles is constant (i.e., there is no net flux of particles). Let $\boldsymbol{U}_r(\boldsymbol{x})$ be the mean velocity of the red particles. Using a prescribed distribution function $f_r(\boldsymbol{c},\boldsymbol{x})$ all the averages $\langle\ \rangle_r$ of any quantity ψ for the red particles can be formed leading to a statistical approach of the phenomenon: $n_r(x)\langle\psi\rangle_r=\int\psi f_r(c,x)dc$.

We aim at predicting the particle dispersion analytically by writing the transport equation of the number density flux $[\boldsymbol{J}_r(\boldsymbol{x})=n_r(\boldsymbol{U}_r-\boldsymbol{U}_p)]$ where $(\boldsymbol{U}_r-\boldsymbol{U}_p)$ is the mean drift velocity of the red particles. n_r, $\boldsymbol{U}_r$, and $\boldsymbol{U}_p$ depend on x. The symbol x is omitted for writing convenience. The balance equation for $\boldsymbol{U}_r$ is obtained by multiplying the Boltzmann equation [Eq. (2)] by c_i and then integrating over the red velocity phase space. Hence, assuming steady state, we can write

$$\frac{\partial}{\partial x_j}(n_r\langle C_iC_j\rangle_r)+\frac{\partial}{\partial x_j}(n_rU_{p,i}U_{r,j})=-n_r\left\langle\frac{c_i-u_i}{\tau_p}\right\rangle_r+C_r(c_i). \tag{4}$$

When both the concentration and the velocity gradients of the red particles are perpendicular to the mean flow direction, the second term on the left-hand side of Eq. (4) reduces to $n_rU_{r,j}\partial U_{p,i}/\partial x_j$. The collisional contribution $C_r(c_i)$ is calculated following the method of [18]. Consequently to any collision of a red particle located at $\mathbf{x}$ and having a velocity $\boldsymbol{c}_A$ with another particle (red or blue) located at $\boldsymbol{x}+2a\boldsymbol{k}$ and having a velocity $\boldsymbol{c}_B$, the expression of the two-particle velocity distribution function $f_r^{(2)}$ can be written for dense suspensions:

$$f_r^{(2)}(\boldsymbol{c}_A,\boldsymbol{x},\boldsymbol{c}_B,\boldsymbol{x}+2a\boldsymbol{k})=g_0f_r(\boldsymbol{c}_A,\boldsymbol{x})\left[f(\boldsymbol{c}_B,\boldsymbol{x})+2ak_m\frac{\partial f(\boldsymbol{c}_B,\boldsymbol{x})}{\partial x_m}\right], \tag{5}$$

where $\boldsymbol{k}$ is the unit vector along the centers line of two colliding particles and a is the particle radius equal for the two particles. Since all the particles have the same physical properties, we can write $f_r(\boldsymbol{c},\boldsymbol{x})$ as a second-order expansion of the mixture equilibrium function f_0:

$$f_r(\boldsymbol{c},\boldsymbol{x})=A_r\left\{1+b_i\frac{\partial}{\partial c_i}+b_{ij}\frac{\partial^2}{\partial c_i\,\partial\,c_j}\right\}f_0(\boldsymbol{c},\boldsymbol{x}). \tag{6}$$

The coefficients A_r, b_i, and b_{ij} are obtained, respectively, by identification of the red particle number density $[n_r=\int f_r(\boldsymbol{c},\boldsymbol{x})d\boldsymbol{c}]$, the mean drift velocity $[n_r(U_{r,i}-U_{p,i})=\int C_if_r(\boldsymbol{c},\boldsymbol{x})d\boldsymbol{c}]$ and the kinetic stress tensor $[n_rT_{ij}=\int C_iC_jf_r(\boldsymbol{c},\boldsymbol{x})d\boldsymbol{c}]$ at a specified location $\boldsymbol{x}$. The three integrals are calculated for $(c_1,c_2,c_3)\in]-\infty,+\infty[$. The coefficients of Eq. (5) are then $[A_r=\frac{n_r}{n}]$, $[b_i=-(U_{r,i}-U_{p,i})]$, and $[b_{ij}=T_{ij}-T\delta_{ij}]$.

The balance equation for the flux $\boldsymbol{J}_r(\boldsymbol{x})$ is obtained by subtracting from Eq. (4) the balance equation written for $\boldsymbol{U}_p$ multiplied by n_r/n. The result after rearrangement is written in the following form:

$$J_{r,k}(\boldsymbol{x})=-(A^{-1})_{ki}T_{ij}\frac{\partial n_r}{\partial x_j}. \tag{7}$$

Recasting Eq. (7) in the classical formulation of Fick's law leads to the definition of a diffusion tensor $[D_{kj}=(A^{-1})_{ki}T_{ij}]$ instead of a single scalar coefficient. A_{ik} is a frequency tensor depending on the characteristic time scales τ_p, τ_c, and γ^{-1}. Its full expression is

$$A_{ik}=\left\{\frac{1}{\tau_p}+\frac{\mathrm{s}}{\tau_c}\right\}\delta_{ik}+\left\{\frac{\partial U_{p,i}}{\partial x_k}-\frac{24}{5}\phi g_0\Pi_{ijkm}\frac{(1+e)}{2}\frac{\partial U_{p,j}}{\partial x_m}\right\} \tag{8}$$

with $[\mathrm{s}=\frac{2}{3}\frac{(1+e)}{2}]$. $[\Pi_{ijkm}=1,\frac{1}{3}]$ when $i=j=k=m$ or two pairs of indices are equal respectively, and $[\Pi_{ijkm}=0]$ in all other cases.

An explicit expression for the self-diffusion tensor for a general flow may be cumbersome. Therefore we shall derive the final results only for a pure shear flow where $[\partial U_1/\partial x_2=\gamma]$. For $[\varphi_a^2-\varphi_b\varphi_c\neq 0]$:

$$D = \frac{1}{\varphi_a^2 - \varphi_b \varphi_c} \begin{pmatrix} \varphi_a & -\varphi_c & 0 \\ -\varphi_b & \varphi_a & 0 \\ 0 & 0 & \dfrac{\varphi_a^2 - \varphi_b \varphi_c}{\varphi_a} \end{pmatrix} \begin{pmatrix} T_{11} & T_{12} & 0 \\ T_{12} & T_{22} & 0 \\ 0 & 0 & T_{33} \end{pmatrix}, \tag{9}$$

with

$$\begin{pmatrix} \varphi_a \\ \varphi_b \\ \varphi_c \end{pmatrix} = \begin{pmatrix} \dfrac{1}{\tau_p} + \dfrac{(1+e)}{3} \dfrac{1}{\tau_c} \\ -\left[\dfrac{8}{5} \phi g_0 \dfrac{(1+e)}{2} \right] \gamma \\ \left[1 - \dfrac{8}{5} \phi g_0 \dfrac{(1+e)}{2} \right] \gamma \end{pmatrix}.$$

In Eq. (9) the shear, collision, and drag contributions are accounted for. Some asymptotic cases of the behavior of particle self-diffusion in a suspension may be discussed:

(i) $\gamma=0$ corresponds to a quiescent fluid flow. The coefficient matrix D becomes diagonal with an isotropic diffusion in the reference axes. The diffusion coefficients are strictly proportional to the normal kinetic stresses with the same prefactor. This is the particular case obtained by [10] $D_{\mathrm{iso}} = [\frac{1}{\tau_p} + \frac{(1+e)}{3}\frac{1}{\tau_c}]^{-1} T$. The constant prefactor (or equivalently $1/\varphi_a$) depends only on the particle relaxation time, the restitution coefficient and the characteristic time between collisions. We note that in a linear shear flow, the self-diffusion coefficient in the spanwise direction D_{33} is the only component that remains simply proportional to the kinetic stress T_{33} with the same prefactor $1/\varphi_a$.

(ii) $\phi \to 0$: In a dilute suspension φ_b vanishes while φ_c tends to γ. Similarly to D_{33} which is proportional to T_{33}, D_{22} becomes proportional to T_{22} ($1/\varphi_a$ being again the constant prefactor). The coefficient D_{11} is always larger; this includes an additional nonzero contribution of the mean shear.

(iii) $\mathrm{St} \to \infty$ or dense suspension: In the regime of highly agitated suspension corresponding to inertial particles or moderate to high suspension concentrations, self-diffusion of the particles is dominated by the occurrence of consecutive collisions (τ_c is the smallest time scale). In this regime, the difference of the normal kinetic stresses is close to zero and the relation $D_{\alpha\alpha} \propto T_{\alpha\alpha}$ becomes similar to the classic prediction of the kinetic theory [9] for dry granular media.

(iv) $\mathrm{St} \to 0$: For dilute and weakly inertial suspensions, the contribution of the drag is dominant because of a short particulate relaxation time, which leads to $D_{\alpha\alpha} \approx \tau_p T_{\alpha\alpha}$. This relation between the self-diffusion coefficient and the velocity fluctuations is a standard view of self-diffusivity. It is similar to Eq. (49) in the work of Brady and Morris [6] when the short-range hydrodynamic forces are dominant and the Brownian agitation negligible. The time scale over which the velocity fluctuation is correlated is τ_p in our case instead of the shear time scale selected by [6]. In the dilute regime, particle encounters will produce a net displacement of the particle across the streamline due to finite inertia. The case of weakly inertial but concentrated suspensions is less obvious as several contributions become significant in Eq. (9). The important contribution of the microstructure included in the term g_0 is similar to the multiplying factor $g^{\infty}(2;\phi)$ emphasized by [6] [Eq. (50)] which becomes dominant in concentrated suspensions.

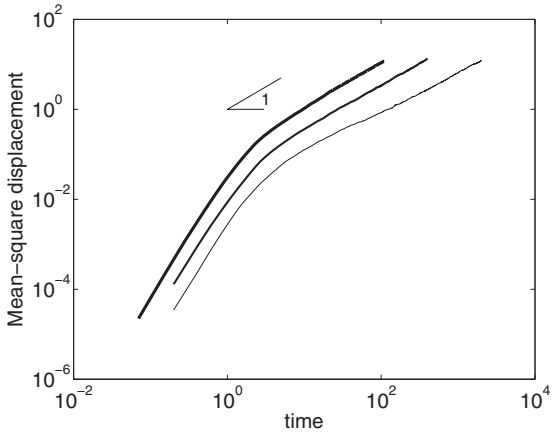

FIG. 3. Mean-square displacement $\langle [x_2(t) - x_2(0)]^2 \rangle / (2a^2)$ vs time ($t\gamma^{-1}$) in log-log scale. The lines correspond to St=1 and $\phi = 5, 15, 30\%$, respectively, from the bottom to the upper line. The slope 1 shows the linear regime of temporal evolution.

B. Validation on simulations

We focus on the validation of the model in the simplified configuration of perfectly elastic particles ($e=1$) suspended in a pure shear flow [$\partial U_{p,1}/\partial x_2 = \gamma$]. The self-diffusion coefficients can be calculated from the simulations based on the trajectories of the particles, using equivalently the long-time temporal evolution of the particle mean-square displacement, the integral of the Lagrangian velocity autocorrelation function, the dynamic structure factor [21], etc. In the present work, the theoretical predictions of diffusion coefficients are compared to the numerical results calculated from the particle mean-square displacement as follows:

$$D_{ij} = \lim_{t \to \infty} \frac{1}{2} \frac{d}{dt} \langle [x_i(t) - x_i(0)][x_j(t) - x_j(0)] \rangle, \tag{10}$$

where $\langle\ \rangle$ is the particle ensemble-average and $\mathbf{x}(0)$ is the particle position at the initial time.

Figure 3 shows the time evolution of the particle mean-square displacement in the shear direction obtained from simulations at St=1. The diffusive regime is reached when the slope of the curve is equal to unity on a logarithmic scale. This corresponds to the loss of Lagrangian velocity autocorrelations as it is shown classically in several studies on self-diffusion [2,3]. We calculated the corresponding self-diffusion coefficient [using Eq. (10)] a long time after the initiation of this linear evolution.

As a first step, we verified the accuracy of Eq. (9) with an *a priori* test. For a given St and ϕ, D_{ij} coefficients are calculated in Eq. (9), using the components T_{ij} obtained from the simulations. Also, τ_c is evaluated from the frequency of particle encounters occurring in our simulations. We used $g_0 = (1 - \phi/\phi_m)^{-2.5\phi_m}$ [22] which tends to infinity when ϕ tends to the maximum packing volume fraction ($\phi_m = 0.64$).

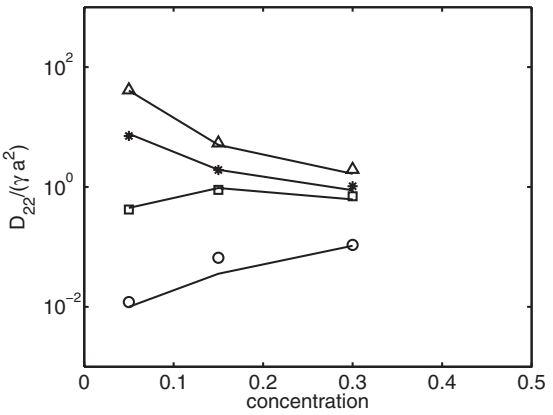

FIG. 4. $D_{22}/\gamma a^2$ vs ϕ. Symbols: numerical results (see Fig. 1). Lines: *a priori* prediction of the model [Eq. (9)] with inputs (T_{ij} and τ_c) from the numerical simulations.

An excellent agreement is observed in Fig. 4, revealing that the theory is relevant provided that the kinetic stress tensor and the collision time are correctly predicted. At high St, the inertial particles diffuse more efficiently for low ϕ where the particle agitation is large and the interparticle distance is wide enough to allow a longer particle mean free path. Increasing ϕ leads to a reduction in self-diffusion. However, the weakly inertial particles diffuse less for low ϕ while they often follow the fluid streamlines. In this quenched regime, diffusion is more efficient when ϕ increases since the particles experience a larger number of collisions induced by the mean flow.

A similar behavior was observed for the self-diffusion in the spanwise direction (Fig. 5). However, D_{33} is not equal to D_{22}, and the difference between both components becomes negligible at high solid concentration for all Stokes numbers. Self-diffusion coefficients related to the flow direction D_{11} and D_{12} were not investigated numerically. Diffusion in the flow direction is coupled to transverse diffusion along the $\mathbf{i}_2$ direction and the mean flow.

The second step consists in comparing the self-diffusion tensor D_{ij} with the full theoretical prediction without any adjustable parameter or any input from the numerical simulations. The theoretical expressions for T_{ij} and τ_c are based on the appropriate (ignited or quenched) theoretical formulations and are now directly used in Eq. (9). The numerical values obtained for the time scale ratio are compared in Fig. 6 with the different expressions based on ignited or quenched state assumptions, respectively. The good agreement observed in this figure is an indicator of a relevant prescription of the time steps used for the different simulations. Figure 7 shows a good agreement between the model using the ignited theory and the numerical simulations when particle inertia prevails (collision regime). When the suspension is weakly agitated, the theoretical prediction fails to predict quantitatively the numerical results on D_{ij}. Especially for St=3.5, the theoretical prediction of D_{22} is significantly underestimated. This is clearly related to the poor prediction of the kinetic theory in this regime (see Fig. 1), since we already verified that the collision time is well predicted by the estimate based on the shear flow (see Fig. 6). Collisions induced by agitation are neglected in the quenched theory. This particular case probably lies in between the fully agitated flow and the fully quenched regime.

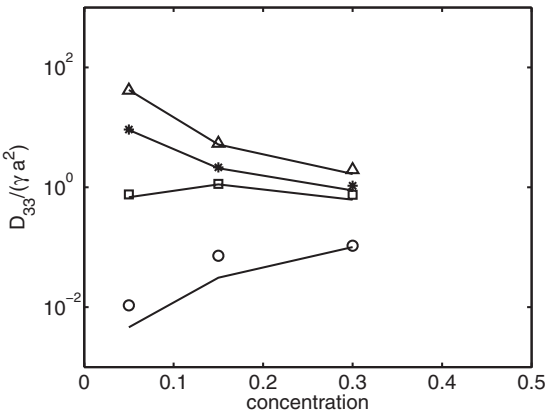

FIG. 5. $D_{33}/\gamma a^2$ vs ϕ. Symbols and lines: same as Fig. 4.

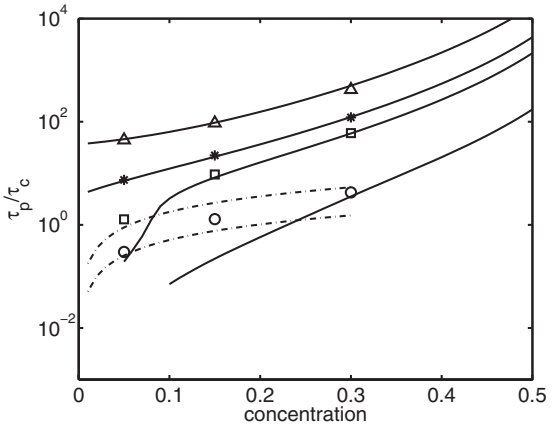

FIG. 6. Time scale ratio τ_p/τ_c vs solid volume fraction for different Stokes numbers. For caption see Fig. 1. The expressions used for the solid and dotted-dashed lines are, respectively, $\tau_c=\frac{a\sqrt{\pi}}{12\phi g_0\sqrt{T}}$ and $\tau_c=\frac{\pi}{16\phi\gamma}$.

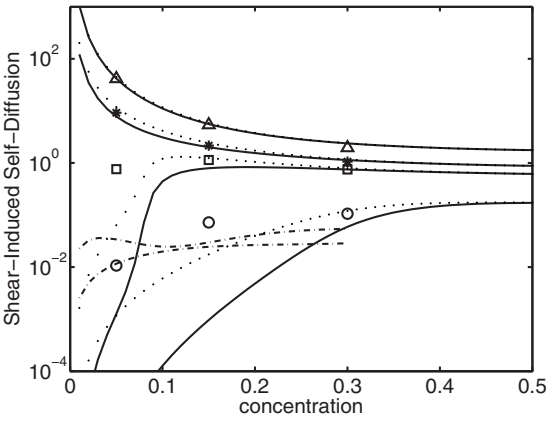

FIG. 7. Self-diffusion coefficient $D_{22}/\gamma a^2$ vs solid volume fraction. Symbols: simulation results (△, ∗, □, ○ correspond, respectively, to St=10, 5, 3.5 and 1). Theoretical predictions [Eq. (9)] using T_{ij} from the ignited (solid lines) and quenched (dotted-dashed lines) theories, respectively, (similar to Fig. 1). Dotted lines: D_{iso} (from top to bottom: St=10, 5, 3.5, and 1).

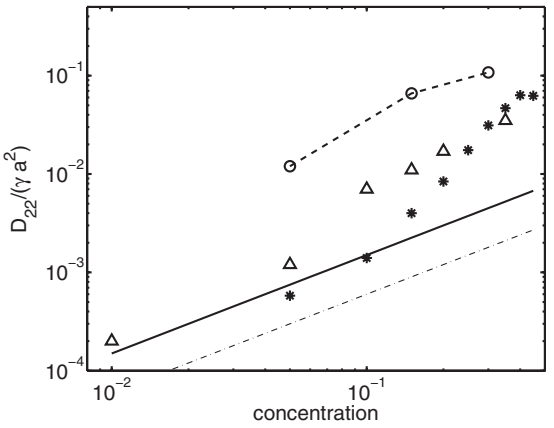

FIG. 8. Comparison of the self-diffusion coefficients $D_{22}/\gamma a^2$ for St=1 with reference results for St$\ll$1. – – ○ – –: our numerical results for St=1. Solid line: theory of [23]. Symbols ∗ and △: results of [21,2], respectively. Thin dotted-dashed line: prediction based on [6].

The numerical result on D_{22} is also compared in Fig. 7 to the self-diffusion coefficient D_{iso} assuming low suspension anisotropy. When the anisotropy is weak (moderate or large ϕ and St), both theoretical predictions are close to the numerical results. Unexpectedly, in some cases of the quenched regime (low ϕ and moderate St), D_{iso} is closer to the simulation results than the general expression D_{22} although the suspension agitation tensor T_{ij} is strongly anisotropic. Indeed, the prediction of D_{22} based on the assumption of a deviated Maxwellian *pdf* (accounting for the anisotropy of T_{ij}) in place of f_0 for D_{iso} (assuming isotropy) overestimated the actual anisotropy (see Fig. 2). Therefore the prediction of D_{22} is less accurate than the simple estimate D_{iso} in this particular intermediate regime.

Finally the self-diffusion coefficients of weakly inertial suspensions (St=1) are compared to theories and simulations valid in the limit St$\to$0 where hydrodynamic interactions are dominant. Since the net displacement following the particle collisions is $O(a)$ in the case St=1, we compare our results on self-diffusivity to theoretical predictions [23] where the particle displacement following a pair interaction is $O(a)$ as well. In Fig. 8, the solid line is the prediction of [23] for the self-diffusivity using the pair trajectory calculations, for a threshold separation length $0.04a$. The linear increase is related to the assumption of pairwise interaction in the dilute regime. Also, the thin dashed line corresponds to $D_{22}/(\gamma a^2\phi)\approx 0.006$ which has been proposed by [6] for a minimum separation distance between the particles equal to $0.04a$. These two predictions only differ by the value of the prefactor which is related to the accuracy of the hydrodynamics pair description. Figure 8 shows that the self-diffusion in suspensions with negligible inertia, St$\ll$1, has the same trend as the weakly inertial suspensions (St=1). However, there is no quantitative agreement between the theoretical values at St$\to$0 and our simulation results at (St=1). For moderate to large concentration, the estimate of self-diffusion coefficients in the dilute regime should be multiplied by the pair distribution function at contact $g^{\infty}(2;\phi)$ which can be a major correction. Figure 8 shows the results obtained by [21] who used the dynamic structure factor method for the determination of self-diffusion characteristics in the limit of negligible Brownian motion. The results of [2] also included in the figure were obtained by numerical simulations using the force coupling method which is based on a low order multipole expansion of the perturbation velocity supplemented by short-range lubrication corrections. All the results shown in Fig. 8 are in good agreement for St$\ll$1 in the dilute regime where the suspension dynamics is controlled by pairwise interactions. In more concentrated suspensions, the multibody interactions increase the resulting particle displacement and enhance self-diffusivity. Our results on weakly inertial suspensions correspond to stronger self-diffusion for all the range of our particulate concentration.

V. CONCLUSION

The long-time behavior of the Lagrangian dispersion of moderately inertial particles has been investigated in the configuration of a pure shear flow. The results of numerical simulations have been compared to a fully theoretical prediction based on the method proposed by [10]. In addition to the classical kinetic theory predictions for the self-diffusion, the effect of the drag force has been taken into account in this work. The self-diffusion tensor was determined as a function of the kinetic stress tensor and the different characteristic time scales related to the shear flow, the collisions, and the viscous relaxation of the particle trajectories. The accuracy of the self-diffusion model was verified by *a priori* tests. An excellent agreement is observed for most cases. Then, simulation results were also compared to the complete theoretical prediction of the self-diffusion coefficients calculated without any adjustable parameter. Similarly to the velocity fluctuations, the self-diffusion of particles depends strongly on the flow regime (quenched or ignited regime depending on the solid concentration and the Stokes number). The self-diffusion coefficients in both the shear and spanwise directions are in good agreement with the theoretical prediction. We showed that the prediction of the self-diffusion tensor is accurate provided that the kinetic stress components are correctly predicted.

ACKNOWLEDGMENTS

Simulations were performed on our regional supercomputing center (Calmip - CICT); they are gratefully acknowledged. The funding of this study was supported by the scientific cooperative federation FERMaT. M.A. acknowledges fruitful discussions with J. F. Parmentier.

[1] J. Wylie, D. Koch, and A. Ladd, J. Fluid Mech. **480**, 95 (2003).
[2] M. Abbas, E. Climent, O. Simonin, and M. Maxey, Phys. Fluids **18**, 121504 (2006).
[3] A. Sierou and J. Brady, J. Fluid Mech. **506**, 285 (2004).
[4] V. Breedveld, D. V. den Ende, A. Tripathi, and A. Acrivos, J. Fluid Mech. **375**, 297 (1998).
[5] A. Acrivos, G. Batchelor, E. Hinch, D. Koch, and R. Mauri, J. Fluid Mech. **240**, 651 (1992).
[6] J. Brady and J. Morris, J. Fluid Mech. **348**, 103 (1997).
[7] S. Chapman and T. Cowling, *The Mathematical Theory of Non-Uniform Gases* (Cambridge University Press, Cambridge, England, 1970).
[8] C. Campbell, J. Fluid Mech. **348**, 85 (1997).
[9] V. Garzo, Phys. Rev. E **66**, 021308 (2002).
[10] J. Lavieville, E. Deutsch, and O. Simonin, in *Proceedings of Sixth International Symposium on Gas-Solid Flows (1995)*, ASME FEDSM Vol. 288, pp. 347–357 (1995).
[11] C. Campbell, Annu. Rev. Fluid Mech. **22**, 57 (1990).
[12] A. Sangani, G. Mo, H. Tsao, and D. Koch, J. Fluid Mech. **313**, 309 (1996).
[13] S. Hsiau and M. Hunt, J. Fluid Mech. **251**, 299 (1993).
[14] S. Hsiau and W. Yang, Phys. Fluids **14**, 612 (2002).
[15] C. Lun and A. Bent, J. Fluid Mech. **258**, 335 (1994).
[16] H. Grad, Pure Appl. Math. **2**, 331 (1949).
[17] C. Lun, S. S. B. Savage, D. Jeffrey, and N. Cherpurniy, J. Fluid Mech. **140**, 223 (1984).
[18] J. Jenkins and M. Richman, Arch. Ration. Mech. Anal. **87**, 355 (1985).
[19] A. Boelle, G. Balzer, and O. Simonin, in *Proceedings of Sixth International Symposium on Gas-Solid Flows (1995)*, ASME FEDSM Vol. 288, pp. 9–18 (1995).
[20] H. Tsao and D. Koch, J. Fluid Mech. **296**, 211 (1995).
[21] A. Leshansky and J. Brady, J. Fluid Mech. **527**, 141 (2005).
[22] C. Lun and S. Savage, Acta Mech. **63**, 15 (1986).
[23] F. DaCunha and E. Hinch, J. Fluid Mech. **309**, 211 (1996).